X-ray investigation of the premartensitic phase in $Ni_{46.8}Ti_{50}Fe_{3.2}$

S. M. Shapiro,* Y. Noda, Y. Fujii, and Y. Yamada
Faculty of Engineering Science, Osaka University, Toyonaka, Osaka 560, Japan
(Received 4 May 1984)

In the shape-memory alloy, NiTi:Fe, the martensitic transformation is well separated from the premartensitic (PM) phase and the latter can be studied in detail. X-ray diffraction studies in the PM phase reveal satellites near $\vec{q}_I=\frac{1}{3}(0,\bar{1},1)$ and $\vec{q}_{II}=\frac{1}{3}(1,1,1)$. For both q values, the satellites are incommensurate and the surprising feature observed is that the incommensurate wave vector $\vec{\delta}$ and the width of the satellites depend upon the Brillouin zone studied. This contradicts a simple condensed charge-density and/or lattice-wave description of the PM phase. If the shift is neglected, the structure in the PM phase can be explained by a condensation of three $[\zeta\bar{\zeta}0]TA_2$ modes with $\zeta=\frac{1}{3}$. In addition we propose a relationship between the well-known ω phase and the PM phase observed in this experiment and for other alloys.

I. INTRODUCTION

Equiatomic NiTi undergoes a martensitic phase transformation at T_M which is near room temperature. Associated with this transition is the novel "shape-memory" effect[1] which can be described as follows. Let the alloy be formed into a particular shape at a temperature $T > T_M$ and then deformed into another shape at a temperature $T < T_M$. Upon heating above T_M, the material returns to its original form, i.e., it "remembers" its shape. The property has several technological applications and is being exploited in the use of many commercially available devices.[2]

Despite the wide applications of NiTi, the underlying physics and metallurgy is far from being understood. It is fair to say that only recently has the structure of the low-temperature martensitic phase been determined.[3] At sufficiently high temperatures, equiatomic NiTi possesses a simple cubic (sc), CsCl-type structure.[4,5] This structure is also referred to as a $B2$ structure and alloys with this high-temperature form are often called β-phase alloys. Several studies in the early 1970s revealed that there were premonitory effects associated with the martensitic transformation.[4,6–9] These premartensitic (PM) effects occur at a temperature only slightly above T_M in pure NiTi. The earlier x-ray-[9] and electron-diffraction[6] studies revealed diffuse streaks and superlattice spots within the PM phase. A recent electron-diffraction study[10] revealed up to seven different diffraction spots in the PM phase. Understanding the origin of the diffraction effects and their connection with the martensitic phase has been the goal of many scientists over the past decade.

Recently, it has been shown that by alloying NiTi with small amounts of Fe, T_M can be suppressed more strongly than the premartensitic transformation.[11] This increases the range of temperatures where the PM phase can be studied without interference from the martensitic transformation. NiTi:Fe has been studied by resistivity,[11] susceptibility,[12] electron-diffraction,[13] x-ray-diffraction,[12] and neutron-diffraction measurements.[14,15] Two well-defined PM transitions occur at T_I and T_{II} as shown in Table I. Superlattice peaks appear below T_I at positions near $\vec{q}_I=\frac{1}{3}(1,\bar{1},0)$ and $\vec{q}_{II}=\frac{1}{3}(1,1,1)$.[12–14] The satellite intensities grow continuously as the temperature is reduced. There is almost no change in the behavior of the β-phase Bragg peaks at T_I. At T_{II} an abrupt splitting of the (111) and (110) Bragg peaks occurs and the system undergoes a rhombohedral distortion which continues to increase as T is reduced.[12,13] At lower temperatures a martensitic transition occurs whose temperature depends strongly upon the iron concentration. Resistivity and specific-heat measurements exhibit a significant change at T_{II} but no change at T_I.[12] The transition at T_I is seen as a change in the slope of magnetic susceptibility.

TABLE I. Transition temperatures in $Ni_{50-x}Ti_{50}Fe_x$ alloys.

	$Ni_{50}Ti_{50}$[a]	$Ni_{47}Ti_{50}Fe_3$[b]	$Ni_{46.8}Ti_{50}Fe_{3.2}$[b–d]
T_I(PM)	293	270	232
T_{II}(PM)		256	224
T_M	273	110	<24

[a]Reference 6.
[b]Reference 12.
[c]Reference 13.
[d]Reference 14.

There have been recent inelastic neutron scattering studies of NiTi (Ref. 16) and NiTi:Fe.[15] Both studies showed anomalies in the $[\zeta\zeta\zeta]$TA and the $[\zeta\zeta 0]$TA$_2$ branches near $\zeta=\frac{1}{3}$ which have been interpreted as being due to electron-phonon interaction.[17] However, only the $[\zeta\zeta 0]$TA$_2$ branch exhibits a strong temperature dependence near $\zeta=\frac{1}{3}$ and suggests that the phase transition is driven by a soft phonon.[15] This low frequency shows up as diffuse scattering in an x-ray- or electron-diffraction study and may be responsible for some of the observed streaks and spots.

The purpose of the present study is to probe the nature of the PM phase by an x-ray-diffraction study of the superlattice peaks appearing below T_I. The main result is that the superlattice peaks are incommensurate with the underlying $B2$ lattice but the magnitude and direction of the incommensurate wave vector do not repeat from one Brillouin zone to another. This precludes a description of the satellites as due to a displacement wave, such as a charge-density wave, arising from a Fermi surface instability. In addition, the $(\frac{1}{3},\frac{1}{3},\frac{1}{3})$ satellites bear a strong resemblance to ω-phase scattering observed in other $B2$ (Ref. 18) and body-centered-cubic (bcc) alloys.[19]

II. EXPERIMENTAL

The x-ray—diffraction experiments were performed on single crystals of $Ni_{46.8}Ti_{50}Fe_{3.2}$ cut from a polycrystalline ingot provided by Raychem Corporation.[20] Etching of the ingot revealed that there were many large grains. These grains were cut from the larger ingot and provided the samples used in the electron-,[13] x-ray-,[12] and neutron-[14,15] diffraction experiments, in addition to the present experiment. Our sample was approximately spherical with a diameter of 0.8 mm. It had a mosaic of 0.2° [full width at half maximum (FWHM)] and the lattice parameter at room temperature is 3.009 Å. The crystal was glued onto a copper post which, in turn, was mounted in a sample container with aluminum foil windows to allow for the entrance and exit of the x-ray beam. The container was placed on the cold finger of a Cryo-Mini Corp. closed-cycle refrigerator. The temperature was computer controlled and regulated to within 0.05 K between 15 and 300 K. Most of the measurements were performed at $T=226$ K which is between T_I and T_{II}, where the basic lattice is still cubic.

The source of x rays was a standard x-ray generator (Toshiba) operated at 20 mA and 40 kV. A copper target was used and a pyrolitic graphite (002) reflection served as a monochromator before the sample. A linear position-sensitive detector was placed 28.7 cm from the sample. It is 50 mm long and the data is divided into 250 channels. Each channel corresponds to an angle of 0.04°. Slits of 0.5 mm width and 1.5 mm height were placed before the sample and that of 8 mm height after the sample. The resolution as determined by mapping of a Bragg peak was approximately 0.01 Å^{-1}. The position-sensitive detector can explore a region of Q space which is 0.33 Å^{-1} on either side of the nominal setting of the spectrometer. The direction in reciprocal space that the counter explores de-

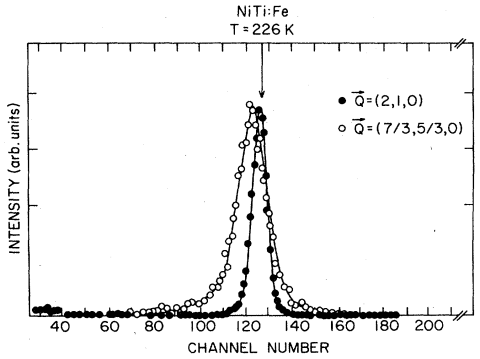

FIG. 1. Intensity vs channel number for the position-sensitive x-ray detector. The arrow indicates the center of the counter which corresponds to the angular setting of the instrument for the chosen Q.

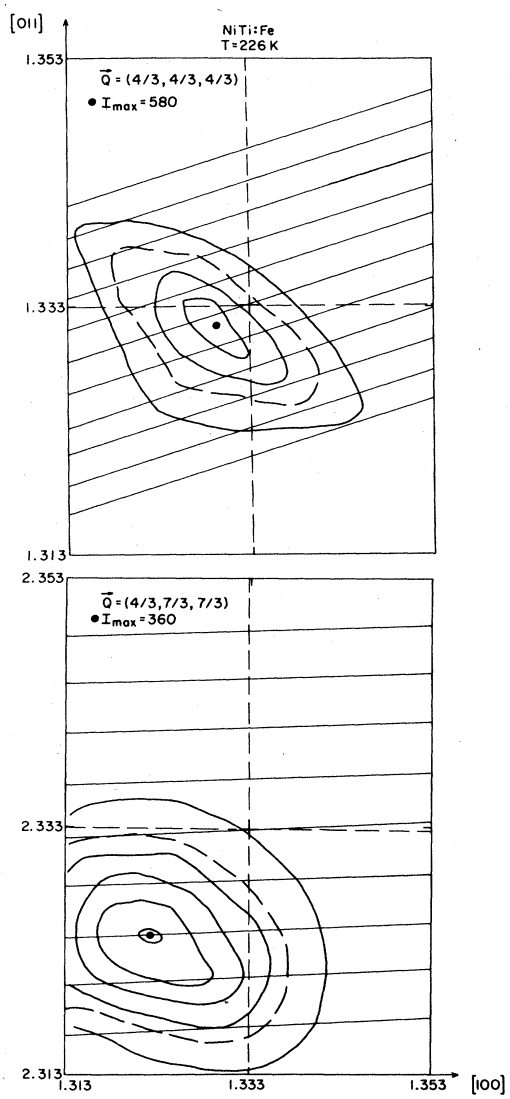

FIG. 2. Equi-intensity contours for two $\vec{q}_{II}$-type satellites. The parallel lines correspond to different settings of the spectrometer. The dashed lines represent half the maximum intensity.

pends upon the scattering vector Q. A program was available which projected the counter onto reciprocal space. This is essential in determining the scan directions in order to map out regions of reciprocal space. Figure 1 shows the intensity recorded in the counter channels for a given spectrometer setting. Intensity contour maps were measured by moving the spectrometer through a particular point of interest in reciprocal space. Figure 2 shows typical intensity contours for NiTi:Fe. The lighter lines running at an angle through each frame correspond to the region spanned by the position-sensitive detector for different settings of the spectrometer. The intensity levels between each setting were interpolated and the subsequent contours were drawn. The dashed lines represent $\frac{1}{2}$ level of intensity.

III. EXPERIMENTAL RESULTS

Satellites are observed near $\vec{q}_{\rm I}=\frac{1}{3}(1,1,0)$ and $\vec{q}_{\rm II}=\frac{1}{3}(1,1,1)$. They appear simultaneously below $T_{\rm I}=232$ K and continue to increase as the temperature is reduced. Figure 1 shows the intensity recorded for the (210) Bragg peak and a $\vec{q}_{\rm I}$-type satellite near $\vec{Q}=(\frac{7}{3},\frac{5}{3},0)$. The arrow corresponds to the center channel of the counter and is the angular setting of the spectrometer for the given Q. In this figure we observe two important features which are characteristic of all the observed satellites: (i) The position of the satellite peak is shifted off of the commensurate position, and (ii) the satellite peak is broader than the resolution-limited Bragg peak. These same features were observed in a neutron study, so surface effects can be ruled out. In order to demonstrate more clearly these effects, intensity contour maps of over 50 satellite positions in both the [001] and [01$\bar{1}$] zones were measured. Intensity contour maps for two $\vec{q}_{\rm II}$-type satellites are shown in Figure 2. It is readily seen that these satellites are not at the commensurate $(\frac{1}{3},\frac{1}{3},\frac{1}{3})$ position, but are shifted by an amount $\vec{\delta}$ towards a smaller wave vector. The unexpected and surprising result is that the amount of incommensurability $\vec{\delta}$ is not the same within each Brillouin zone as it would be if the incommensurability were due to a displacement wave. Figure 2 also reveals that the width is aniostropic and elongated along the [11$\bar{2}$] direction which is perpendicular to [111]. The width, too, increases with Q.

Figures 3 and 4 show the intensity contours for the measured $\vec{q}_{\rm I}$- and $\vec{q}_{\rm II}$-type satellites, respectively. The positions of the satellites were corrected for spectrometer misalignments by forcing the nearby Bragg peaks to be on the correct positions. Typical corrections were on the order of $0.002a^*$ ($a^*=2\pi/a$). The pluses (+) in the figures denote the commensurate $\frac{1}{3}$ positions. The Q scale for each box is magnified by a factor of 10. The dashed lines correspond to the intensity contour at half the maximum intensity. The intensity contours are shown for the (210) Bragg peak in Fig. 3 and the (200) Bragg peak in Fig. 4 which represents the instrumental resolution.

Schematic representations of the observations are shown in Figs. 5 and 6 for the (001) and (01$\bar{1}$) zones, respectively. In these figures the length of the arrows is not significant but the direction shows the direction of

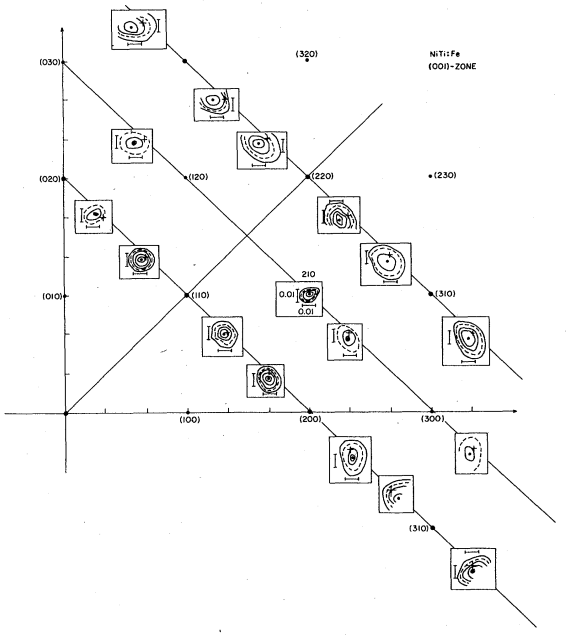

FIG. 3. Observed intensity contours in the (001) zone showing the $\vec{q}_{\rm I}$-type satellites. Each box is magnified and the bar represents $0.01a^*$ units. The cross corresponds to the commensurate $\frac{1}{3}$ position. The dashed lines are at half the maximum intensity. The (210) Bragg peak represents the instrumental resolution.

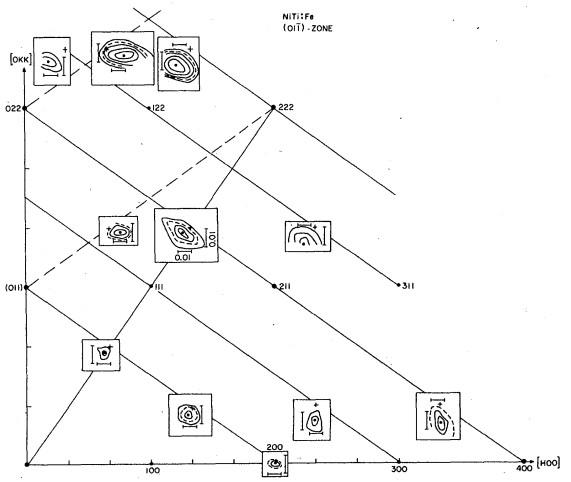

FIG. 4. Observed intensity contours in the (0$\bar{1}$1) zone show the $\vec{q}_{\rm II}$-type satellites. Each box is magnified and the bar represents $0.01a^*$ along $[H00]$ and $0.01\sqrt{2}\ a^*$ along $[0KK]$. The plus corresponds to the commensurate $\frac{1}{3}$ position. The dashed lines in the contours are at half the maximum intensity. The contours along the dashed lines correspond to the domain associated with the [$\bar{1}$11] direction.

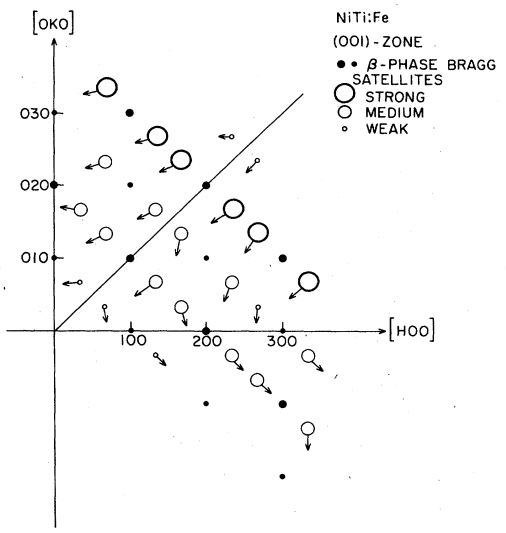

FIG. 5. Schematic representation of observed satellites in the (001) zone. The arrows indicate the direction of the incommensurate wave vector, but their length is not significant.

$\vec{\delta}(Q)$. There is a definite pattern to the $\vec{q}_I=\frac{1}{3}(1,1,0)$-type satellites. The more intense satellites are along the $[1\bar{1}0]$ rows which correspond to the rows of intense Bragg peaks. This implies a transverse type of modulation with $\vec{q}_I$ parallel to $[1\bar{1}0]$ and displacements along the [110] direction. There is no systematic behavior of the $\vec{q}_{II}$-type satellites readily determined from Fig. 4 or 6.

The scattering vector for each satellite can be defined as

$$\vec{Q}=\vec{\tau}+\vec{q}_c+\vec{\delta}\,, \tag{1}$$

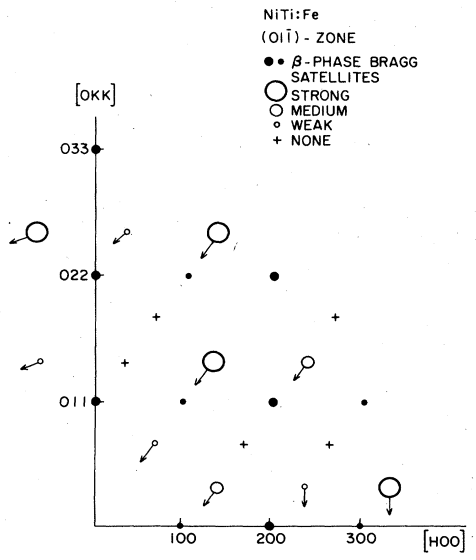

FIG. 6. Schematic representation of observed satellites in the $(01\bar{1})$ zone. The arrows indicate the direction of the incommensurate wave vector, but their length is not significant.

where $\vec{\tau}$ is a reciprocal-lattice vector, $\vec{q}_c$ is the reduced wave vector measured from $\vec{\tau}$ to the commensurate $\frac{1}{3}$ position, and $\vec{\delta}$ is the measure of the amount of incommensurability. In the results presented in Figs. 3—6, we see that $\vec{\delta}$ depends upon which Brillouin zone is being probed, i.e., $\vec{\delta}=\vec{\delta}(\vec{Q})$. The trend is that $\vec{\delta}$ increases with $\vec{Q}$. This is clearly seen in Fig. 2 where two $\vec{q}_{II}$-type satellites are compared. Also, the linewidth increases with increasing $\vec{Q}$. This is seen in Fig. 4 by comparing the $(\frac{4}{3},\frac{1}{3},\frac{1}{3})$ satellite, which is nearly resolution limited, to the $(\frac{4}{3},\frac{7}{3},\frac{7}{3})$ satellite which is about four times the size of the resolution. Additionally, the direction of $\vec{\delta}(Q)$ changes with $\vec{Q}$. This is revealed in Figs. 5 and 6, which show that the $\vec{\delta}$'s point generally towards smaller $\vec{Q}$. For satellites along the [111] direction (Fig. 6), $\vec{\delta}(Q)$ is nearly parallel to [111], whereas for $\vec{Q}=(\frac{10}{3},\frac{1}{3},\frac{1}{3})$, $\vec{\delta}$ is closer to the [011] direction and for $\vec{Q}=(\frac{2}{3},\frac{7}{3},\frac{7}{3})$, $\vec{\delta}$ is nearly parallel to [100]. The pattern of the $\vec{\delta}(Q)$ for $\vec{q}_I$-type satellites (Fig. 5) is symmetrical about the [110] direction. The pattern is a counterclockwise "swirl" for $H>K$ and a clockwise swirl for $K>H$.

IV. DISCUSSION

A. Approximate structure in PM-I phase

The most surprising result of the present experiment is the $\vec{Q}$ dependence of the incommensurate wave vector $\vec{\delta}$. This rules out the description of the superlattice as being due to a modulated wave represented by a single wave vector, such as a charge-density wave (CDW) resulting from Fermi surface effects.[21] The $\vec{Q}$ dependence of $\vec{\delta}$ suggests that local effects which break the translational symmetry play an important role in the transition. Yamada *et al.*[22] proposed a model based upon a modulated lattice relaxation to explain the observed shifts of the satellites.

However, the approximate structural characteristics in the premartensitic phases should be present in the overall distribution of intensities of these satellites within reciprocal space. In order to investigate the approximate structure, let us momentarily neglect the shift of the satellite positions as well as broadening of the spectra and simply assume that there develops a long-range order characterized by the commensurate wave vectors $\vec{q}_I=\frac{1}{3}(1,1,0)$ and $\vec{q}_{II}=\frac{1}{3}(1,1,1)$. We then consider a possible static structure which is consistent with the observed overall intensity distribution of these commensurate satellites, or superlattice spots. The temperature where extensive observations were carried out was $T=226$ K, which is between T_I and T_{II}. Therefore, in the following we restrict our discussion to the structure at PM-I phase.

The key consideration is that neutron scattering results[15,16] showed that a softening of the [110]TA_2-phonon mode occurs near $\vec{q}=\frac{1}{3}(1,1,0)$. This strongly suggests that the phase transition at T_I is primarily associated with the TA_2-phonon mode with $\vec{q}=\frac{1}{3}(1,1,0)$. We notice that there are six degenerate modes belonging to the "star" of the equivalent wave vectors within the first Bril-

louin zone. The static structure would be derived from a linear combination of these degenerate modes. We further notice that below T_{II} the system transforms to rhombohedral lattice with the [111] cubic axis parallel to the rhombohedral unique axis.

We, therefore, introduce three phonon modes with the wave vectors perpendicular to the [111] axis and with transverse polarization $\vec{e}$,

$$\vec{q}_I^{(1)}=\tfrac{1}{3}(1,\bar{1},0),\quad \vec{e}_1\|[110]\,,$$
$$\vec{q}_I^{(2)}=\tfrac{1}{3}(0,1,\bar{1}),\quad \vec{e}_2\|[011]\,, \qquad (2)$$
$$\vec{q}_I^{(3)}=\tfrac{1}{3}(\bar{1},0,1),\quad \vec{e}_3\|[101]\,,$$

and take the following linear combination to construct the displacements of the kth atom:

$$\vec{U}_k=\eta\sum \vec{e}_i\cos(\vec{q}_I^{(i)}\cdot\vec{r}_k+\phi)\,, \qquad (3)$$

where η is the amplitude of the modulation wave, and ϕ is the phase factor.

The phase was chosen as $\phi=0$ to give the cosine factor in Eq. (3). The displacements of the atoms are shown in Fig. 7 as seen looking down the [111] direction. Figure 7(a) shows the atomic positions projected on the (111) plane and the right side shows the stacking of the planes along the [111] direction. Figure 7(b) shows the displacement calculated using Eqs. (2) and (3) with an arbitrarily chosen η and $\phi=0$. The left portion of the figure gives the shifts of the atoms in planes perpendicular to [111]. The symmetry of the phase with these displacements is $P3lm$ and the unit cell is shown in Fig. 7(a) with lattice parameters a_{PM} and b_{PM}. If the phase factor ϕ is chosen as $\pi/2$, then the symmetry becomes $P\bar{3}$ with the same unit cell. In Table II we list the lattice vectors for this phase and the reciprocal-lattice vectors. $\vec{a}_{PM}$ is along the $[11\bar{2}]$ direction and the reciprocal-lattice vector is $\frac{1}{3}(0,1,\bar{1})$. Thus, the satellites observed in the (001) plane would be Bragg peaks of a phase with the new trigonal lattice, if complete long-range order were present. Similarly, the $\frac{1}{3}(1,1,1)$ peaks are Bragg peaks along the new c direction. The existence of the satellites is due to a trigonal structure which is driven by a soft mode with wave vectors of Eq. (2).

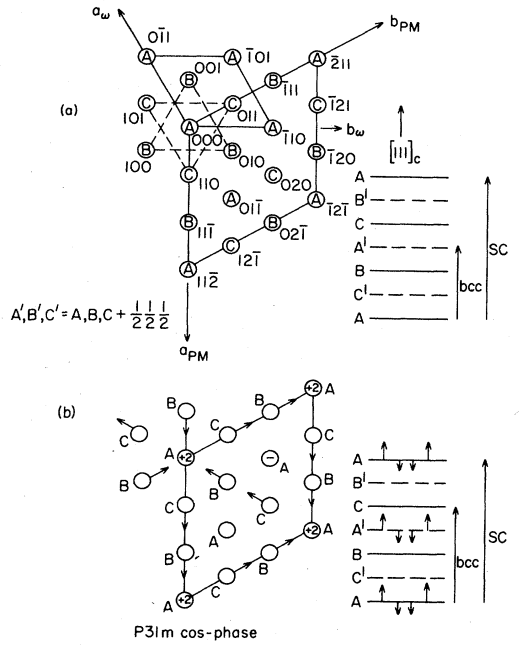

FIG. 7. (a) Atomic positions of CsCl structure as viewed down the [111] direction. The Miller indices correspond to atomic positions using cubic notation. The atoms with the same letters are in the same plane, perpendicular to [111]. The right side shows the stacking sequence of the planes parallel to [111]. (b) Atomic displacements of atoms determined by three transverse phonons with wave vector $|\vec{q}|=\frac{1}{3}(0,\bar{1},1)$ using Eq. (3). The left side has the [111] direction perpendicular to the plane of the page and the right side shows the displacements parallel to [111].

Once the atomic displacements are obtained it is straightforward to calculate the expected x-ray intensity using the equation

$$I(\vec{Q})=\left[\frac{1+\cos^2 2\theta}{2}\right]\left|\sum_k f_k e^{i[\vec{Q}\cdot(\vec{r}_k+\vec{U}_k)]}\right|^2, \qquad (4)$$

TABLE II. Lattice vectors of trigonal phase derived from soft mode of cubic phase (cubic indices). $m=\frac{1}{2}$ for sc lattice, 1 for bcc lattice; $n=\frac{1}{3}$ for sc lattice, $\frac{2}{3}$ for bcc lattice.

Wave vector of phonon	$\frac{1}{3}(1,\bar{1},0)$	$\frac{1}{3}(1,1,\bar{2})$
Direction of displacements	[110]	[111]
Real-space lattice vectors	$\vec{a}=(1,1,\bar{2})$	$\vec{a}=(\bar{1},1,0)$
	$\vec{b}=(\bar{2},1,1)$	$\vec{b}=(0,\bar{1},1)$
	$\vec{c}=m(1,1,1)$	$\vec{c}=m(1,1,1)$
Reciprocal-lattice vectors	$a^*=\frac{1}{3}(0,1,\bar{1})$	$a^*=\frac{1}{3}(\bar{2},1,1)$
	$b^*=\frac{1}{3}(\bar{1},1,0)$	$b^*=\frac{1}{3}(\bar{1},\bar{1},2)$
	$c^*=n(1,1,1)$	$c^*=n(1,1,1)$

where the angular prefactor takes into account the polarization of the x rays and f_k is the scattering power. The displacements are taken from Eqs. (3). The results are shown in a qualitative way in Fig. 8 for the two zones studied. Absorption has not been taken into account, but this would reduce the intensity of the smaller Q satellites more than the larger Q satellites. There is no significant difference of the calculated intensity on (001) and (011) planes between two model structures deduced by choosing $\phi=0$ and $\pi/2$.

Considering the absorption, the agreement between the observed Fig. 5 and calculated Fig. 8 intensities in the [001] zone is quite reasonable. Generally, intense satellites are observed near strong Bragg peaks and weak satellites near weak Bragg peaks. In the [011] zone the agreement is not as good. The calculated intensity shows that the $(\frac{2}{3},\frac{5}{3},\frac{5}{3})$ satellite should be as intense as the $(\frac{4}{3},\frac{4}{3},\frac{4}{3})$ position. This is not what is observed since the $(\frac{2}{3},\frac{5}{3},\frac{5}{3})$ peak is absent in the experiment. This disagreement in the (011) zone tells us that we do not completely understand the mechanism producing the $\frac{1}{3}(111)$-type satellites.

It is interesting to notice that the pattern of the $\vec{q}_{II}$ satellite intensities observed in the [011] zone is very similar to what is observed in Zr and Ti metals alloyed with V, Nb, or Ta. These alloys show a metastable low-temperature omega (ω) phase[23] which is a trigonal phase corresponding to the motion of two adjacent (111) planes of the parent bcc phase moving towards each other. Liu *et al.*[19] performed a mapping of the diffuse x-ray intensity in the (011) zone for several compositions of the alloy $Zr_{1-x}Nb_x$. In Table III we compare the observed peak intensity[19] for Zr—12 wt% Nb to our observations in NiTi:Fe. In both cases the $(\frac{4}{3},\frac{4}{3},\frac{4}{3})$ satellite is the strongest and the $(\frac{5}{3},\frac{5}{3},\frac{5}{3})$ is absent. In the Zr-Nb study, as the Nb concentration increases the satellites become broader and are elongated perpendicular to the [111] direction. The other major observation was that the shifts of the ω-phase peaks are all towards the origin and that the shift varies from zone to zone. These features are precisely what is observed in the present experiment on NiTi:Fe. Similar observations were noted on a $Ni_{53.8}Al_{46.2}$ (Ref. 18) alloy which has a CsCl structure.

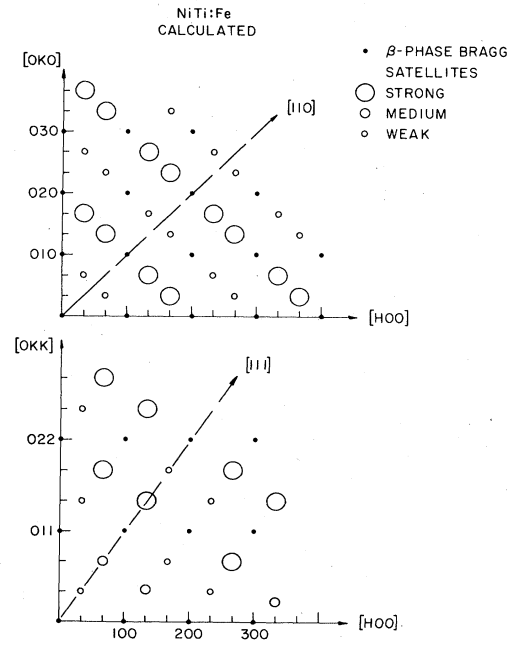

FIG. 8. Calculated x-ray intensities for [001] and [01$\bar{1}$] zones using the displacement pattern given in Fig. 7. These intensities are to be compared with observed intensities of Figs. 3 and 4.

TABLE III. Comparison between peak intensity of $(\frac{1}{3},\frac{1}{3},\frac{1}{3})$-type satellites of NiTi:Fe with ZrNb (arbitrary units). *, not measured.

$\vec{Q}=(h,k,l)$	NiTi:Fe	ZrNb(2%) (Ref. 19)
$(\frac{4}{3},\frac{4}{3},\frac{4}{3})$	580	590
$(\frac{4}{3},\frac{7}{3},\frac{7}{3})$	350	100
$(\frac{2}{3},\frac{7}{3},\frac{7}{3})$	200	150
$(\frac{10}{3},\frac{1}{3},\frac{1}{3})$	120	*
$(\frac{4}{3},\frac{1}{3},\frac{1}{3})$	70	*
$(\frac{2}{3},\frac{4}{3},\frac{4}{3})$	60	100
$(\frac{2}{3},\frac{2}{3},\frac{2}{3})$	25	<13
$(\frac{1}{3},\frac{7}{3},\frac{7}{3})$	30	<13

Summarizing the above, we have shown that the $\vec{q}_I$- and $\vec{q}_{II}$-type satellites are approximately interpreted as Bragg peaks of a low-temperature trigonal structure caused by the triple condensation of the phonons along the $[\zeta\bar{\zeta}0]TA_2$ branch at $\zeta=\frac{1}{3}$.

B. Relationship with other β-phase materials

We now propose a relationship between the present observations and phase transitions in other β-phase materials. Phonon anomalies which exhibit strong temperature dependencies are expected to be the origin of the transitions in β-phase alloys. The major anomalies occur either in the longitudinal acoustic branch near $q=\frac{2}{3}(1,1,1)$ or in the transverse $[\zeta\bar{\zeta}0]TA_2$ branch with polarization along [110]. It should be noted that the $\frac{2}{3}(1,1,1)$-LA point is equivalent to the $\frac{1}{3}(1,1,\bar{2})$ transverse mode with polarization along [111]. Thus there are two transverse modes with propagation directions perpendicular to the [111] directions which are important in the phase transitions in the β-phase alloys. Nagasawa *et al.*[23] recognized the importance of the "special mode" corresponding to the transverse $[11\bar{2}]$ mode, but they restricted their discussion to the zone center. Likewise, Tanner *et al.*[24] tabulated several alloys which undergo a martensitic transformation and exhibit a softening in the C' elastic constant.

The structure of the low-temperature phase is determined by which branch exhibits a stronger anomaly and the degeneracy of the mode. First, we consider the case when a minimum occurs at the $\frac{1}{3}(\bar{1},\bar{1},2)TA$ point. Displacements of atoms are derived from the phonon mode:

$$\vec{q}_{II}^{(1)}=\tfrac{1}{3}(\bar{1},\bar{1},2),\quad \vec{e}\,||\,[111]\,. \tag{5a}$$

We notice that, in contrast to the case of $\vec{q}_I$-mode condensation, the modes

$$\vec{q}_{II}^{(2)}=\tfrac{1}{3}(2,\bar{1},\bar{1}),\quad \vec{e}\|[111]\,,$$
$$\vec{q}_{II}^{(3)}=\tfrac{1}{3}(\bar{1},2,\bar{1}),\quad \vec{e}\|[111]\,, \tag{5b}$$

which are generated by threefold symmetry operation, are essentially equivalent to $\vec{q}_{II}^{(1)}$, as shown in Fig. 9. Hence, any linear combination of the three modes is simply reduced back to the single-mode condensation.

The symmetry is either $P3ml$ or $P\bar{3}ml$, depending on the choice of the cosine function or sine function as the phase factor. The c direction of this trigonal phase is along the [111] direction and the unit cell of this phase is shown in Fig. 7(a) with lattice vectors given as $\vec{a}_\omega$ and $\vec{b}_\omega$. The unit cell is smaller than that obtained with the choice of wave vectors of Eq. (2). The relation between the lattice vectors is given in Table II. Notice that all the new Bragg peaks of this phase are at reduced positions of $\frac{1}{3}(1,1,1)$. In order to compare with Eq. (3), we take a triple $\vec{q}_{II}$ representation. The displacement pattern generated using

$$U_k=\eta\sum_{i=1}^{3}\vec{e}_i\sin(\vec{q}_{II}^{(i)}\cdot\vec{r}_k) \tag{6}$$

gives motion only along the [111] direction. The atoms in the B and C' planes of Fig. 7 move towards each other as do the atoms in the C and B' planes. This motion is that which takes the cubic phase into the ω phase.[25] This is borne out in Zr and Ti alloys which are known to exhibit ω phases.[26] An enhanced minimum appears at the $\frac{2}{3}(1,1,1)$-LA point in the host lattice. Measurements along the $[\zeta\bar{\zeta}0]TA_2$ branch show less of an anomaly.

On the other hand, if an anomaly occurs in the $[\zeta\bar{\zeta}0]TA_2$ branch then a structure different from ω phase will be present [Fig. 7(a)]. For an anomaly occurring at $\vec{q}_I=\frac{1}{3}(1,\bar{1},0)$ there are several possible structures arising from the degeneracy of the mode. When the three modes are condensing simultaneously (triple $\vec{q}_I$ condensation) the new phase has another trigonal-type structure which we have discussed in Sec. III. According to the discussions, satellites appear at $\frac{1}{3}(1,1,0)$ in addition to $\frac{1}{3}(1,1,1)$.

When the phase transition is associated with a single $\vec{q}_I$-mode condensation, the new phase belongs to the orthorhombic system. Other β-phase alloys exhibit this type of phase transition. Among these are AgCd, AuCd,[27] and $AuCuZn_2$,[28] where mostly $\frac{1}{3}(1,1,0)$-type satellites were studied, and NiAl,[18] where only $\frac{1}{3}(1,1,1)$-type satellites were studied. The dispersion curves have been measured in only a few alloys: $AuCuZn_2$,[29] CuAlNi,[30] and CuZnAl,[31] but mostly along the $[1\bar{1}0]$ direction. In CuZnAl Guenin *et al.*[31] measured along the $[11\bar{2}]$ direction and they showed that there was no minimum at $\frac{1}{3}(1,1,\bar{2})$ and the low-temperature transition is determined by the dynamics of the $[1\bar{1}0]$ branch. In none of the above-mentioned alloys have the satellite intensities been mapped out in as much detail as in the present example of NiTi:Fe. It is planned to probe the diffuse scattering of some of these alloys and see if features are present which are similar to what is reported here.

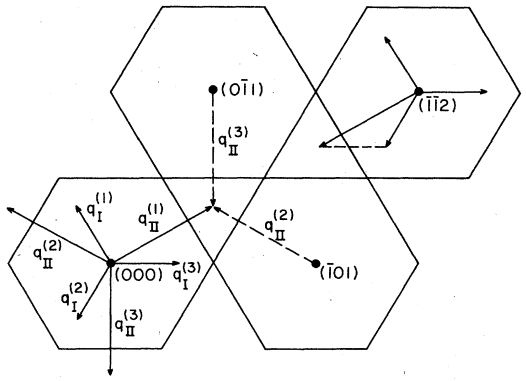

FIG. 9. Formation of "star" of $\vec{q}_I$'s and $\vec{q}_{II}$'s. In the case of $\vec{q}_{II}$'s the degeneracy due to the star is superfluous because these wave vectors are reduced into a single $\vec{q}$ as represented by dashed arrows. Also, notice that $\vec{q}_{II}^{(1)}=\vec{q}_I^{(3)}-\vec{q}_I^{(2)}$.

V. CONCLUSIONS

The study of NiTi:Fe has yielded interesting new results on the nature of the martensitic phase transitions in alloys. We observe an incommensurate phase whose incommensurability depends upon the Brillouin zone studied. The presence of two types of satellite peaks, observed in many other β-phase alloys, is explained as a condensation of a transverse $[\zeta\bar{\zeta}0]TA_2$ phonon with $\zeta=\frac{1}{3}$.

ACKNOWLEDGMENTS

One of us (S.M.S.) wishes to express gratitude to the Yamada Science Foundation for the grant which enabled him to visit Japan. He also expresses his appreciation to students in the Yamada Laboratory who assisted in this research. We are also indebted to J. D. Axe, P. Bak, J. Krumhansl, M. Meichele, M. Salamon, L. Tanner, and G. Vineyard for many helpful discussions. Work at Brookhaven National Laboratory was supported by the Division of Materials Sciences, U.S. Department of Energy, under Contract No. DE-AC02-76CH00016.

*Permanent address: Department of Physics, Brookhaven National Laboratory, Upton, NY 11973.

[1]W. J. Buehler, J. V. Gilfrich, and R. C. Wiley, J. Appl. Phys. **34**, 1475 (1963).
[2]L. McDonald Schethy, Sci. Am. **241**, 82 (1979).
[3]W. Bührer, R. Gotthardt, A. Kulik, O. Mercier, and F. Staub, J. Phys. F **13**, L77 (1983).
[4]K. Chandra and G. R. Purdy, J. Appl. Phys. **39**, 2176 (1968).
[5]A. Nagasawa, J. Phys. Soc. Jpn. **31**, 136 (1971).
[6]G. D. Sandrock, A. J. Perkins, and R. F. Heheman, Metall.

Trans. 2, 2769 (1971).
[7]F. E. Wang, S. J. Pickart, and H. A. Alperin, J. Appl. Phys. **43**, 97 (1972).
[8]D. P. Dautovich and G. R. Purdy, Can. Metall. Q. **4**, 129 (1965).
[9]K. Otsuka, T. Sawamura, and K. Shimizu, Phys. Status Solidi **5**, 457 (1971).
[10]G. M. Michal, P. Moine, and R. Sinclair, Acta Metall. **30**, 125 (1982).
[11]M. Matsumoto and T. Honma, Trans. Jpn. Inst. Met. Suppl. **17**, 199 (1976).
[12]M. Meichle, Ph.D. thesis, University of Illinois, 1981.
[13]C. M. Hwang, M. Meichle, M. B. Salamon, and C. M. Wayman, Philos. Mag. A **47**, 9 (1983); **47**, 31 (1983).
[14]M. B. Salamon, M. Meichle, C. M. Wayman, C. M. Hwang, and S. M. Shapiro, in *Modulated Structures—1979 (Kailua Kona, Hawaii)*, proceedings of the International Conference on Modulated Structures, AIP Conf. Proc. No. 53, edited by J. M. Cowley, J. B. Cohen, M. B. Salamon, and B. J. Wuensch (AIP, New York, 1979), p. 223.
[15]S. K. Satija, S. M. Shapiro, M. B. Salamon, and C. M. Wayman, Phys. Rev. B **29**, 6031 (1984).
[16]W. Bührer, V. Mercier, P. Brüesch, and R. Gotthardt, Eidgenössische Technische Hochschule Zürich Report No. AF-SSP-115, 1981 (unpublished), p. 60.
[17]R. Bruinsma, Phys. Rev. B **25**, 2951 (1982).
[18]P. Georgopoulos and J. B. Cohen, Acta Metall. **29**, 1535 (1981).
[19]W. Lin, H. Spalt, and B. W. Batterman, Phys. Rev. B **13**, 5158 (1976).
[20]Raychem Corporation, 300 Constitution Drive, Menlo Park, CA 94025.
[21]J. D. Axe, Philos. Trans. R. Soc. London, Ser. B **290**, 593 (1980).
[22]Y. Yamada, Y. Noda, M. Takimoto, and K. Furukawa (unpublished).
[23]A. Nagasawa, N. Nakanishi, and K. Enami, Philos. Mag. A **43**, 1345 (1981).
[24]L. Tanner, R. A. Pelton, and R. Gronsky, J. Phys. (Paris) Colloq. **43**, C4-169 (1982).
[25]B. S. Hickman, J. Mater. Sci. **4**, 554 (1969); H. E. Cook, Acta Metall. **23**, 1041 (1975); R. Pynn, J. Phys. F **8**, 1 (1978); T. S. Kuan and S. L. Sass, Acta Metall. **24**, 1053 (1976); B. Horovitz, J. L. Murray, and J. A. Krumhonel, Phys. Rev. B **18**, 3549 (1978).
[26]C. Stassis, J. Zaretsky, and N. Wakabayashi, Phys. Rev. Lett. **41**, 1726 (1978).
[27]A. Nagasawa, J. Phys. Soc. Jpn. **40**, 1021 (1976).
[28]A. Nagasawa, K. Mizunoya, N. Nakanishi, K. Enami, and S. Nenno, Scr. Metall. **12**, 409 (1978).
[29]M. Mori, Y. Yamada, and G. Shirane, Solid State Commun. **17**, 127 (1975); R. A. Robinson, G. L. Squires, and R. Pynn, J. Phys. F **14**, 1061 (1984).
[30]S. Hoshino, G. Shirane, M. Suezawa, and T. Kajitani, Jpn. J. Appl. Phys. **14**, 1233 (1975).
[31]G. Guénin, D. Rios Jara, M. Morin, L. Delaey, R. Pynn, and P. F. Goben, J. Phys. (Paris) Colloq. **43**, C4-597 (1982). R. Pynn (unpublished) also observed satellites whose incommensurability varied with Brillouin zone.